J. Fluid Mech. (1984), *vol.* 141, *pp.* 51–66
Printed in Great Britain

Numerical computation of time-dependent Taylor-vortex flows in finite-length geometries

By G. P. NEITZEL

Department of Mechanical and Aerospace Engineering, Arizona State University, Tempe, Arizona 85287

(Received 18 August 1983 and in revised form 16 November 1983)

The time-dependent Navier–Stokes equations are integrated numerically for a finite-length concentric-cylinder geometry. The motion is initiated by an impulsive start of the inner cylinder from a state of rest. The transient development of a Taylor-vortex structure is discussed from the standpoint of the amplitude history, the onset time and vortex-front propagation; steady-state results are compared with previously published experimental results.

1. Introduction

All laboratory flows occur in finite geometries and, moreover, are time-dependent to some extent (if only by virtue of their starting conditions). Basic understanding in fluid mechanics has now developed to the point where it is reasonable to attempt a study of the influence of these non-classical effects on the stability characteristics of various flows. A good deal of attention has been focused on these effects in recent years. A popular candidate for various stability theories and experiments has been flow between concentric rotating cylinders. The reasons for this popularity are threefold: namely that the character of the geometry and the basic states makes the corresponding stability problem somewhat amenable to analysis, experiments are relatively easy to perform, and there is a great deal of experience with the successes (and failures) of infinite-cylinder models. The classical consequence of instability in this flow is the appearance of a periodic Taylor-vortex structure. Modern research is concerned with modifications to this structure due to finite cylinder length and/or time-dependent cylinder motion.

Experimentalists have long made use of time-dependent cylinder motions and variable-length annuli to achieve states other than the one reached by increasing the inner-cylinder speed in a quasi-steady manner from a subcritical state. Coles (1965), for instance, was able to find as many as twenty-six stable states existing at a single Reynolds number. Benjamin and Mullin (Mullin 1982; Benjamin & Mullin 1982) have performed experiments in annuli of modest aspect (length-to-gap) ratio, obtaining at least 39 steady flows. Among these are the so-called 'anomalous modes' for which cells adjacent to the annulus endwalls spiral in the 'wrong' direction. They have also studied transitions between what they term the 'primary flow' (that which is realized by gradual increases in inner-cylinder angular velocity from small values) and secondary flows that result from further increases in angular velocity. A summary of some recent theoretical efforts to account for finite-length effects may be found in the review article by DiPrima & Swinney (1981). Time dependence may be either periodic in nature or aperiodic, such as an impulsive change in a boundary motion.

The former are discussed by Davis (1976); references to work on flows with basic states which are aperiodic in time (impulsive and non-impulsive) may be found in Neitzel (1982*a*).

Experiments in a concentric-cylinder geometry for which time-dependence and finite length are both important were performed by Burkhalter & Koschmieder (1974). They measured the wavelengths of steady-state vortices that resulted from impulsively starting the inner cylinder from a state of rest. The outer cylinder was held fixed, and various end conditions and aspect ratios γ were employed; tests were performed for a wide range of supercritical Reynolds (or Taylor) numbers. They found that the average wavelength of the interior vortices (excluding those at the ends which are driven by Ekman pumping) initially decreased with increasing Reynolds number R, reaching a minimum plateau for $3 \leqslant R/R_c \leqslant 4$, where R_c denotes the infinite cylinder, linear-stability theory critical Reynolds number. For $R/R_c > 4$, the wavelength was found to increase with increasing R. The aim of the present work is to examine this problem from the standpoint of a set of numerical experiments.

Meyer (1967) computed Taylor-vortex flows from Couette-flow initial states by assuming axial periodicity (i.e. an infinite cylinder) and imposing initial disturbances of specified axial wavelength. Alonso & Macagno (1973) performed similar computations. Alziary de Roquefort & Grillaud (1978) computed slightly supercritical flows in finite-length annuli by increasing the Reynolds number in several small increments, as might an experimentalist, allowing the flow to reach steady state between increments. Meyer-Spasche & Keller (1980) solved the steady, axisymmetric Navier–Stokes equations using Fourier expansions in the axial direction and a pseudoarclength continuation method to trace the bifurcation from circular Couette flow to Taylor-vortex flow.

The above computations have been concerned with the stability of steady flow between concentric rotating cylinders. An unsteady basic state was considered by Liu & Chen (1973), who performed numerical experiments for sudden starts, assuming an axially periodic flow and superposing random initial disturbances. Neitzel & Davis (1981) conducted numerical experiments for spin-down within single cylinders of finite length using a semi-implicit finite-difference technique to integrate the time-dependent Navier–Stokes equations, allowing instabilities to be triggered by round-off and truncation errors. Of interest here were the onset times of instabilities and the effects of the instability on such quantities as spin-down times. It is the numerical method employed by Neitzel & Davis which has been adapted to treat the problem of interest here. The details will be presented in §2.

The object of the present work is to compare the results of the computations with the steady-state measurements of Burkhalter & Koschmieder (1974) and, in addition, to examine various aspects of the onset process itself. From the numerical experiments of Alziary de Roquefort & Grillaud (1978) it is known that the transition to Taylor-vortex flow in a finite geometry is a smooth one, beginning with Ekman cells at each endwall for small subcritical Reynolds numbers and ending with toroidal vortices filling the entire annulus ($\gamma = 10$) for $R/R_c = 1.17$. Prior to this point, it was noted that cells appeared in the vicinity of the midplane, as is observed for the more strongly nonlinear flows computed here. These features are also seen in laboratory experiments. A recent paper by Ahlers & Cannell (1983) discusses the onset within finite cylinders in terms of a propagating vortex front. We shall present results of a vortex-front velocity computed for a few of the cases treated here.

The numerical simulation allows us to study finite-geometry impulsively initiated flows such as these, tracing the development of disturbances to finite values.

Certainly, such flows even within infinite cylinders are untreatable by present-day linear-stability theories (Homsy 1973; Neitzel 1982*b*), and energy theory, while yielding lower bounds on onset times, cannot provide any information about the approach to a secondary equilibrium state. All these difficulties are in addition to those encountered in determining the basic state, if indeed it can be determined at all. Therefore it appears that, for flows of this type, numerical experimentation is the only theoretical tool at our disposal at this time.

2. Formulation

Consider a pair of concentric circular cylinders of radii a and b and height h. We assume the gap between the cylinders to be filled with a viscous incompressible fluid of kinematic viscosity ν. The entire system is assumed to be in an initial state of rest. At time $t' = 0$, the inner cylinder at radius $r' = a$ is impulsively set into rotation with angular velocity Ω while the outer cylinder at $r' = b$ is held fixed. The rigid endwalls at $z' = 0, h$ are assumed to be attached to the inner cylinder and therefore begin to rotate with it at $t' = 0$. Burkhalter & Koschmieder (1974) have also considered fixed endwalls and a free surface, but we shall not do so here.

The governing equations for axisymmetric flow may be written in dimensionless form as:

$$\Gamma_t + \frac{1}{r}\psi_z\Gamma_r - \frac{1}{r}\psi_r\Gamma_z = \frac{1}{R}\left[\nabla_1^2\Gamma - \frac{1}{r}\Gamma_r\right], \tag{2.1a}$$

$$\zeta_t + \frac{1}{r}\psi_z\zeta_r - \frac{1}{r}\psi_r\zeta_z - \frac{u\zeta}{r} - \frac{2}{r^3}\Gamma\Gamma_z = \frac{1}{R}\left[\nabla_1^2\zeta + \frac{1}{r}\zeta_r - \frac{1}{r^2}\zeta\right], \tag{2.1b}$$

$$\nabla_1^2\psi - \frac{1}{r}\psi_r = r\zeta, \tag{2.1c}$$

where

$$\nabla_1^2 = \frac{\partial^2}{\partial r^2} + \frac{\partial^2}{\partial z^2}. \tag{2.1d}$$

The velocity components are (u, v, w) in the directions given by the cylindrical coordinates (r, θ, z). Here the circulation is proportional to Γ,

$$\Gamma \equiv rv, \tag{2.1e}$$

the stream function ψ in the (r, z)-plane is given by

$$u \equiv \frac{1}{r}\psi_z, \quad w \equiv -\frac{1}{r}\psi_r, \tag{2.1f}$$

and ζ, the θ-component of vorticity, is given by

$$\zeta \equiv u_z - w_r. \tag{2.1g}$$

The variables have been made dimensionless using the scales $d \equiv b-a$, Ωd and Ω^{-1} for length, speed and time respectively. The Reynolds number R is defined to be

$$R = \Omega d^2/\nu \tag{2.2}$$

and the aspect ratio γ is

$$\gamma = h/d. \tag{2.3}$$

Since we are dealing with symmetric end conditions we reduce the size of the computational domain by assuming the flow to be symmetric about the midplane

at $z = \frac{1}{2}\gamma$. This restricts the flow to have an even number of vortices, which is the case normally observed in the laboratory (ruling out, of course, the anomalous modes of Benjamin & Mullin 1982). Under the assumptions of axial and midplane symmetries and for rotating endwalls, the boundary conditions for system (2.1) are as follows:

$$\psi = 0, \quad \Gamma = \frac{\eta^2}{(1-\eta)^2}, \quad \zeta = \left(\frac{1}{\eta} - 1\right)\psi_{rr} \quad \text{at} \quad r = \frac{\eta}{1-\eta}, \tag{2.4a}$$

$$\psi = 0, \quad \Gamma = 0, \quad \zeta = (1-\eta)\psi_{rr} \quad \text{at} \quad r = \frac{1}{1-\eta}, \tag{2.4b}$$

$$\psi = 0, \quad \Gamma = r^2, \quad \zeta = \frac{1}{r}\psi_{zz} \quad \text{at} \quad z = 0, \tag{2.4c}$$

$$\psi = 0, \quad \Gamma_z = 0, \quad \zeta = 0 \quad \text{at} \quad z = \tfrac{1}{2}\gamma. \tag{2.4d}$$

The initial condition is a state of rest, so that

$$\psi = \Gamma = \zeta = 0 \quad \text{for} \quad t < 0. \tag{2.5}$$

In (2.4), $\eta = a/b$ is the radius ratio, which was set for these computations to the value $\eta = 0.727$ to match one of the experimental configurations of Burkhalter & Koschmieder (1974).

System (2.1) with boundary conditions (2.4) and initial conditions (2.5) were solved numerically using the techniques employed previously by Neitzel & Davis (1981) to study spin-down. A more complete discussion of the code appears there and in a paper by Kitchens (1980), who originally developed the code to study spin-up, and will not be repeated here. Briefly, the stream-function equation (2.1*c*) is solved using a Gauss–Seidel method, while the circulation and vorticity equations were solved by a semi-implicit predictor–corrector–multiple-iteration (PCMI) technique, which treats the radial direction implicitly and the axial direction iteratively.

Both Neitzel & Davis and Kitchens made use of grid-stretching transformations in one or more coordinate directions to place more grid points near solid boundaries. For the problem considered here, the vortices eventually fill the entire annulus, both radially and axially. Therefore good resolution is required everywhere in the flow field, and, for this reason, constant grid spacing was used. Through numerical experimentation it was decided for the case $\gamma = 23.35$ that 18 radial points and 199 axial points were sufficient for the range of Reynolds numbers considered. Therefore the distances between points in the radial and axial directions were essentially the same since only half of the axial extent need be computed.

3. Results and discussion

The computations described in the previous section were done on the Arizona State University IBM 3081 computer using double-precision arithmetic. A maximum of 10 iterations were allowed for convergence of the stream function, and up to 25 iterations were allowed for the PCMI solutions of the vorticity and circulation equations. Computation time was of the order of half a millisecond per grid point per iteration of the PCMI procedure. The results of every fifth time step were written to tape for later analysis.

Numerical experiments were performed for several cases of impulsive starts from rest. Burkhalter & Koschmieder (1974) used various cylinder lengths for their

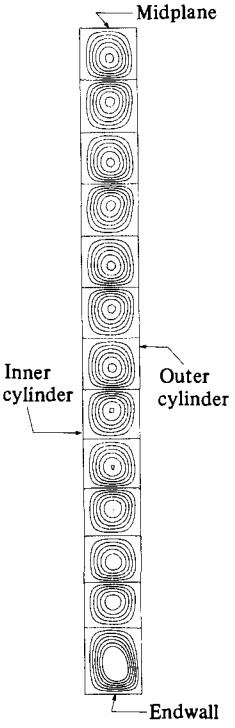

FIGURE 1. Steady-state vortex pattern for $R = 62.06$ and $\gamma = 23.35$ at $t = 140$.

experiments, observing variations of interior-cell (i.e. excluding endcells) wavelengths which exhibited strong dependence on Reynolds number, but appeared to be relatively insensitive to changes in aspect ratio. For this reason and for considerations of economy, we confine attention here to aspect ratios near the lower end of the range considered by Burkhalter & Koschmieder. Flows were calculated for an aspect ratio of $\gamma = 23.35$, which corresponds exactly to the smallest of the experimental values, and a few cases were also considered for $\gamma = 22$.

3.1. *Steady-state results*

The experiments of Burkhalter & Koschmieder (1974) were primarily concerned with the steady-state flow that is established following a sudden start. In particular, we shall compare our numerical results for endcell size and interior-cell wavelength to their results. Results will be presented both in terms of R/R_c, and, for convenience of comparison, T/T_c, which is the same ratio for the Taylor number; as defined, the latter ratio is the square of the former.

Assuming that the size of the endcells is dictated more by the presence of rotating endwalls than by overall apparatus length, the average wavelength of the interior vortices is quantized owing to the fact that only an integral number of cell pairs may be observed. Thus one would not expect the average wavelengths of interior cells in apparati of two different aspect ratios γ_1 and γ_2 to coincide, unless the difference $|\gamma_1 - \gamma_2|$ is equal to an integral number of these wavelengths.

Figure 1 shows instantaneous streamlines for the steady-state flow resulting from an impulsive start to $R = 62.06$. For radius ratio $\eta = 0.727$, $R_c = 31.03$, so that this case corresponds to $R/R_c = 2$ and $T/T_c = 4$. One may easily see the effect of the

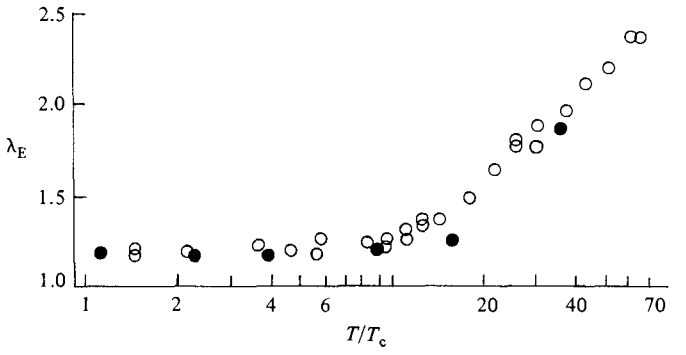

FIGURE 2. Endcell size versus Taylor number (rotating endwalls): ○, Burkhalter & Koschmieder (1974) laboratory results; ●, present numerical experiments.

rotating endwall on the cell adjacent to it. This cell is driven primarily by Ekman pumping (Greenspan 1968) and is present at any value of Reynolds number, although not necessarily of the size found here. For $R/R_c = 0.0039$ and $\gamma = 10$, Alziary de Roquefort & Grillaud (1978) show a weak endcell penetrating all the way to the midplane. This cell develops almost immediately after the start of the rotation – the Ekman layer is established within two radians, according to Benton & Clark (1974). In the present computations, the endcell appears early and changes only slightly during the approach to steady state. A comparison between the endcell sizes determined numerically and those measured experimentally may be found in figure 2. As plotted here, λ_E is the size of single endcell, scaled by d. The numerical values of λ_E are calculated by taking the mean of the endcell boundary ($\psi = 0$) locations determined one grid point into the flow from the inner and outer cylinders respectively. In agreement with laboratory results, the size of the endcell from the numerical experiments remains relatively constant up to $T/T_c = 9$, and then increases although not as rapidly as in the laboratory experiments. Notice that the predicted endcell size for $T/T_c = 36$ is in quite good agreement with the laboratory results, indicating that the disagreement between predicted and measured interior-cell wavelengths for this case is not attributable to a poor prediction of endcell size.

Interior-cell wavelengths λ_{eff} plotted in figure 3 are determined by subtracting endcell sizes from the aspect ratio and dividing the result by the number of interior vortex pairs N, i.e.

$$\lambda_{eff} = \frac{\gamma - 2\lambda_E}{N}. \tag{3.1}$$

It should be emphasized that λ_{eff} is a measure of the average wavelength of interior cells after the flow has reached a steady-state configuration. Agreement between experimentally and numerically determined values of λ_{eff} is excellent for $1 < T/T_c \leqslant 16$. λ_{eff} is seen to decrease with increasing T/T_c in this range. However, the numerical results for $T/T_c = 36$ ($R/R_c = 6$) show a departure from the trend observed experimentally. As stated in the previous paragraph, this lack of agreement is due to an incorrect prediction of the number of interior cells, not to an error in the prediction of λ_E. For strongly supercritical starts, the earliest-appearing vortex pattern does not persist indefinitely. This was observed in the laboratory experiments of Kirchner & Chen (1970) as well as in the present calculations. Figure 4 shows instantaneous streamline patterns computed for $R/R_c = 6$ at three different times

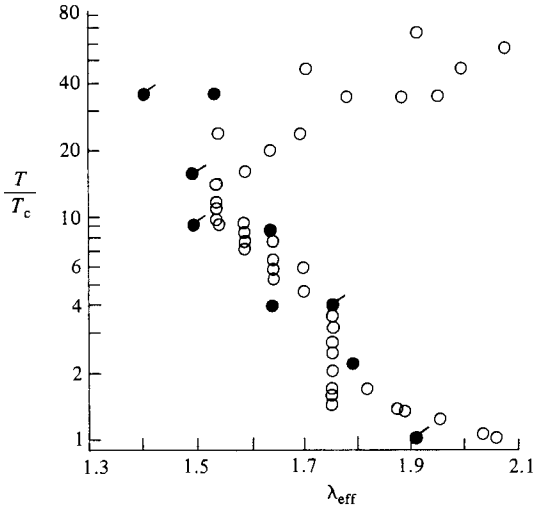

FIGURE 3. Interior-cell effective wavelength: ○, Burkhalter & Koschmieder (1974); ●, numerical experiments, $\gamma = 22$; ●, numerical experiments, $\gamma = 23.35$.

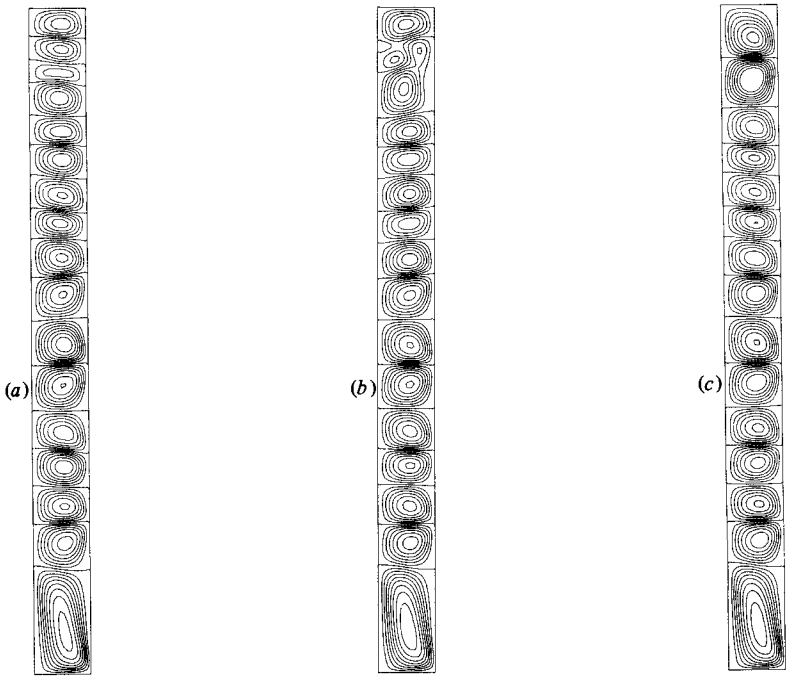

FIGURE 4. Instantaneous streamlines for $R/R_c = 6$ at three times: (*a*) $t = 40$; (*b*) 56; (*c*) 60.

during which the flow was changing from a 17-cell (in the computational space) configuration to one with 15 cells. As seen in the last of these plots, the interior-cell size is quite non-uniform. Barring further changes in the number of cells, one would expect the pattern to equilibrate in size on a diffusive timescale associated with the length h of the apparatus. Snyder (1969) has shown experimentally that the

dimensional relaxation time for such a system of vortices is approximately $h^2/6\nu$. In terms of the dimensionless time employed here, this corresponds to $t \approx 1.7 \times 10^4$ for $R = 186.18$ and $\gamma = 23.35$. Our computation was continued to $t = 380$ (only 2.2% of Snyder's relaxation time), and, while the cells were not yet of equal size, it did not appear that further changes in the number of interior cells were likely.

Another explanation for the failure of the code to predict the number of interior cells accurately for this case is the possible influence of non-axisymmetric effects. While the steady flow observed experimentally may have been axisymmetric, it is possible (and even likely) that during the transient phase, wavy modes may have been important. Since ours is an axisymmetric computation, it is unable to account for the presence of these wavy modes and is therefore unable to properly predict the flow in such a regime. The agreement between the numerical and laboratory experiments for $R/R_c \leqslant 4$, however, gives us confidence in the ability of the code to yield useful information regarding the development of axisymmetric instabilities.

3.2. *Transient effects*

The development of finite-amplitude Taylor vortices from small initial disturbances is a complicated nonlinear phenomenon even for the case of a steady weakly nonlinear basic state. This development for such a basic state in an infinite geometry is usually described by the so-called Landau equation

$$\frac{dA}{dt} = \sigma A - bA^3, \tag{3.2}$$

where $A(t)$is the amplitude of the disturbance, σ is the linear-theory growth rate, and b is the 'Landau constant', which for circular Couette flow is positive. The solution of (3.2), for $A(0) < (\sigma/b)^{\frac{1}{2}}$, exhibits the initial exponential growth expected on the basis of linear-stability theory, followed by equilibration to an amplitude

$$A_e = (\sigma/b)^{\frac{1}{2}} \tag{3.3}$$

as t becomes infinite. Excellent agreement between theory and experiments for weakly nonlinear Couette flows has been obtained by Donnelly, Schwarz & Roberts (1965). For strongly nonlinear flows in finite geometries, no such theory exists for comparison with our numerical experiments. One would expect, however, that the *initial* disturbance development would resemble Landau-type behaviour.

Any number of measures might be used to denote the disturbance amplitude $A(t)$. Since the numerical experimentalist has the advantage of being able to view the entire experiment before deciding where to take data, one might choose to monitor the axial component of velocity midway (in an axial sense) between two points where the boundaries of a single cell will appear in the steady-state flow. The 'probe' could be positioned radially near the point of maximum axial velocity in the vortex on either the inner-cylinder or outer-cylinder side. The initial axial velocity should be quite small, if one stays away from an endwall, and a change in its magnitude is indicative of the growth of an instability to the nearly pure swirl basic state. This was done at a couple of locations for some of the cases considered here. The results are independent of position insofar as the initial onset of growth and qualitative development of the disturbance are concerned, but, as one would expect, the equilibrium amplitude A_e is dependent on probe location. Another consideration is that, since the apparatus is of finite length, cells are observed to move slightly in the axial direction as they adjust to changes in the number of cells and as they begin to equilibrate in size. Such shifting will cause changes in the velocity at a fixed point

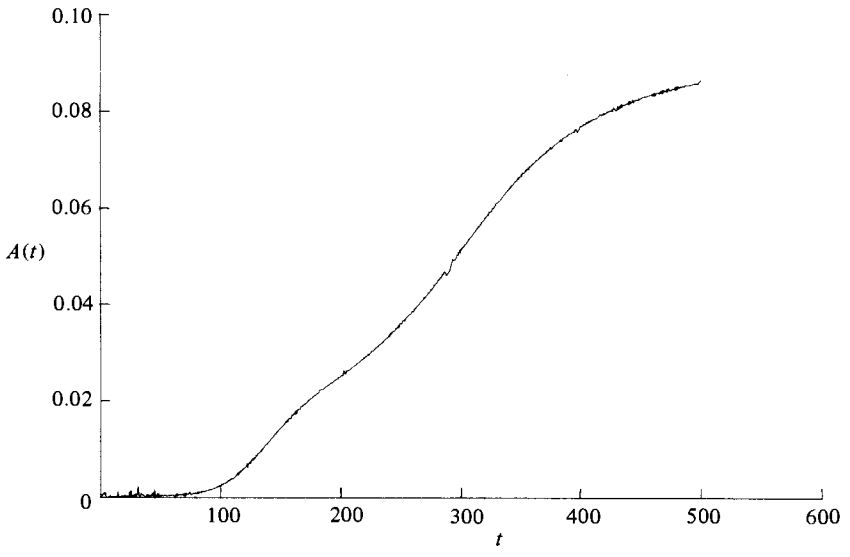

FIGURE 5. Amplitude history for $R/R_c = 1.03$.

in the laboratory reference frame which may or may not be indicative of the overall strength of a cell. For these reasons, we chose to seek an alternative measure of $A(t)$.

Since we have the stream function ψ in the (r, z)-plane at our disposal, and since $\psi_a - \psi_b$ is equal to the volume flow rate between streamlines passing through two points a and b in the flow field, we can compute the strength of an individual vortex by taking the difference between $\psi_{\max}$, the maximum value of ψ within the vortex, and the value of ψ on the boundary of the vortex ($\psi = 0$). Such a measure is global (for one cell) rather than local, and therefore more difficult to determine in a laboratory experiment, but it has the advantage of being independent of position (once a particular cell is identified) and insensitive to slight axial motion of the cell. It is, of course, still arbitrary in the sense that a particular cell must be selected. For the computations performed here, the cell adjacent to the midplane was selected. This cell is easily identified numerically (being adjacent to the boundary of the computational domain), and sometimes begins to appear early due to spontaneous nucleation near the midplane. We therefore define our $A(t)$ to be

$$A(t) = \psi_{\max,\,\text{computed}}|_{\text{midplane cell}}, \tag{3.4}$$

where the subscripted 'computed' refers to the fact that the maximum value computed for any grid point is used rather than fitting a surface through $\psi(r, z)$ and determining the maximum value of ψ on the surface. This was done to reduce computation time, and, while this will undoubtedly introduce some noise into the results, the results should be representative of $A(t)$ due to the density of grid points used (roughly 18×18 per cell).

Figures 5–9 show the behaviour of $A(t)$ as a function of time for $1.03 \leqslant R/R_c \leqslant 6$ and $\gamma = 23.35$. All curves exhibit the type of initial growth characteristic of solutions of (3.2), but quickly lose that character as the amplitude becomes larger. The computation for $R/R_c = 1.03$ (figure 5) was extended to $t = 500$ without $A(t)$ reaching what might be called A_e. The pattern is changing only insofar as cells in the interior regions are becoming more nearly equal in strength to their neighbours closer to the

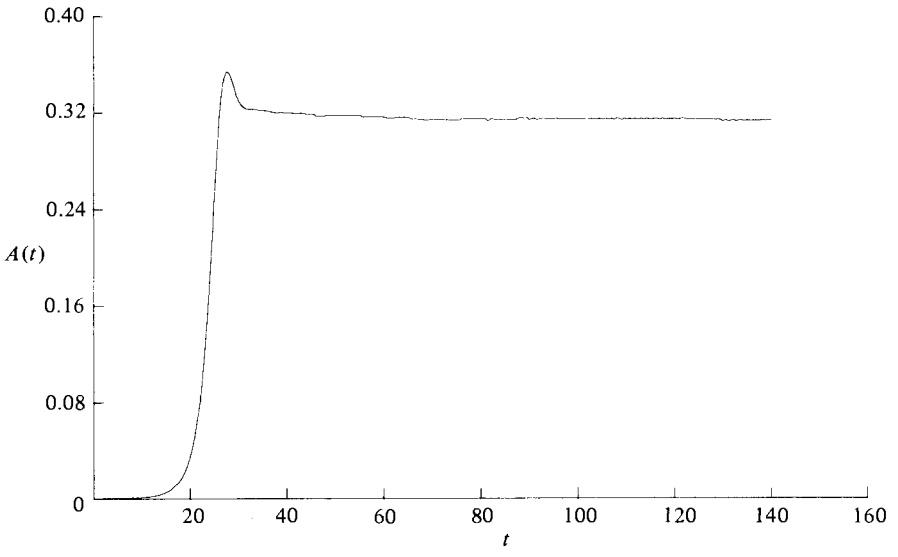

FIGURE 6. Amplitude history for $R/R_c = 2$.

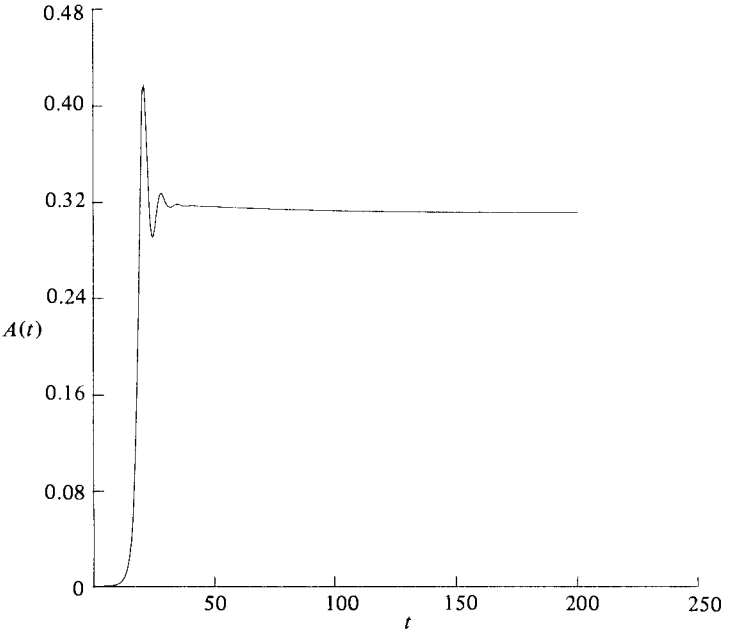

FIGURE 7. Amplitude history for $R/R_c = 3$.

ends. For $2 \leqslant R/R_c \leqslant 4$ (figures 6–8), there is a region of rapid growth to an amplitude which overshoots A_e followed by a recovery to A_e. The amount of oscillation following the overshoot increases with increasing R/R_c. This same type of behaviour was observed when examining the time history of the axial velocity at a point, as discussed earlier.

One possible explanation for this overshoot is the spontaneous nucleation of cells near the midplane. What we have observed as spontaneous nucleation near the

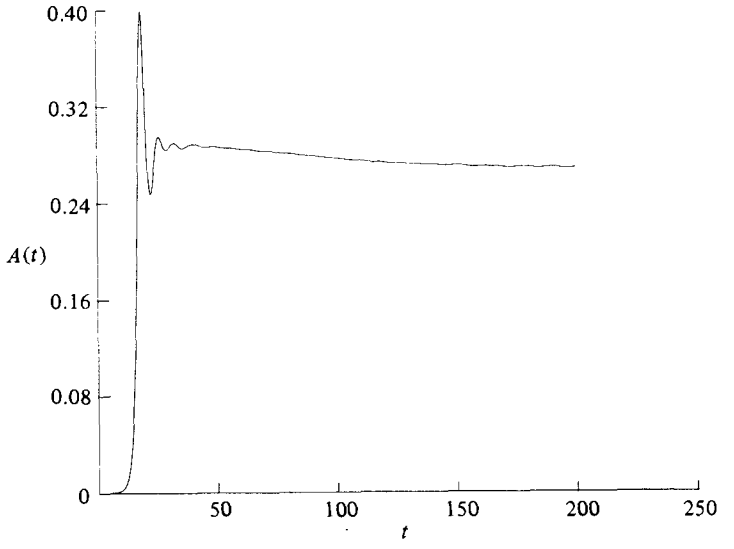

FIGURE 8. Amplitude history for $R/R_c = 4$.

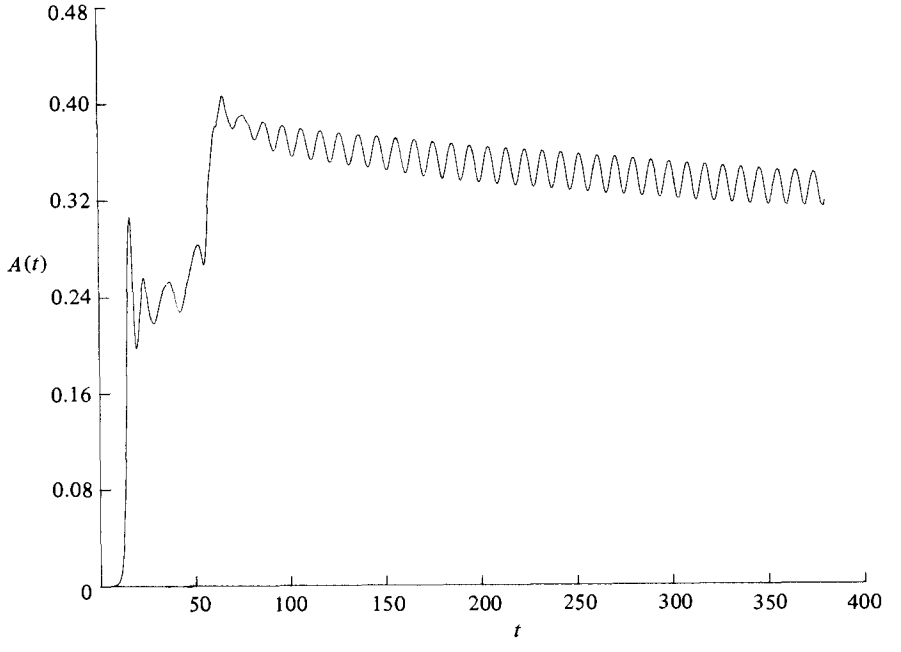

FIGURE 9. Amplitude history for $R/R_c = 6$.

midplane in these computations is undoubtedly due, in part, to the imposition of a symmetry boundary there and to the iterative nature of the solution procedure, which sweeps in the axial direction. However, one does observe nucleation in the interior regions during laboratory experiments not unlike that seen here. Figure 10 shows streamline plots for $R/R_c = 2$ at two times during the establishment of the pattern. One can see not only the propagation of vortices from the endwall into the interior

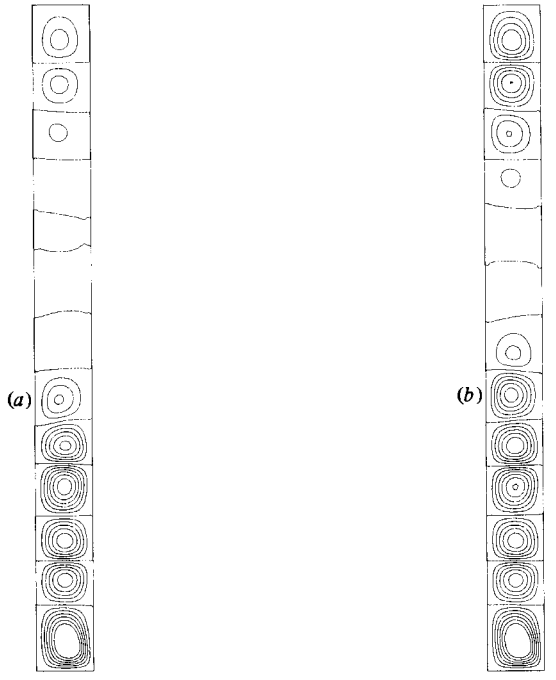

FIGURE 10. Instantaneous streamlines for $R/R_c = 2$ at two times showing nucleation near the midplane and vortex front propagation: (*a*) $t = 23$; (*b*) $t = 25$.

R/R_c	A_e	t_Ω	t_D	t_B	t_E
1.03	0.087	233.70	7.303	10.81	1.769
2	0.314	22.85	0.3682	2.427	0.124
3	0.311	17.40	0.1869	1.729	0.077
4	0.268	15.27	0.1230	1.403	0.059
6	0.32	13.61	0.0731	1.081	0.043

TABLE 1. Onset-time results for $\gamma = 23.35$

but also the development of cells near the midplane. At time $t = 23$ the two cells at the midplane are the strongest of this group, while at $t = 25$ the cells adjacent to them have increased in strength, partly at the expense of the first pair. Notice that these changes are occurring during the same time period where we see the overshoot in $A(t)$ (figure 6).

Finally, in figure 9 we see the amplitude history for $R/R_c = 6$. Recall that this is the case whose value for λ_{eff} disagreed sharply with the data of Burkhalter & Koschmieder (1974). Here, instead of approaching some A_e following the initial overshoot and subsequent oscillation, there is a second increase in A in the vicinity of $t = 50$, followed by oscillations which remain nearly constant in peak-to-peak amplitude. The second rise appears during the time period discussed previously when the flow undergoes a reduction in the number of cells (see figure 4). The persistent oscillations may be associated with an instability of this new flow which cannot take place due to the restriction of axisymmetry. It is clear that our numerical simulation cannot properly describe the flow for this case.

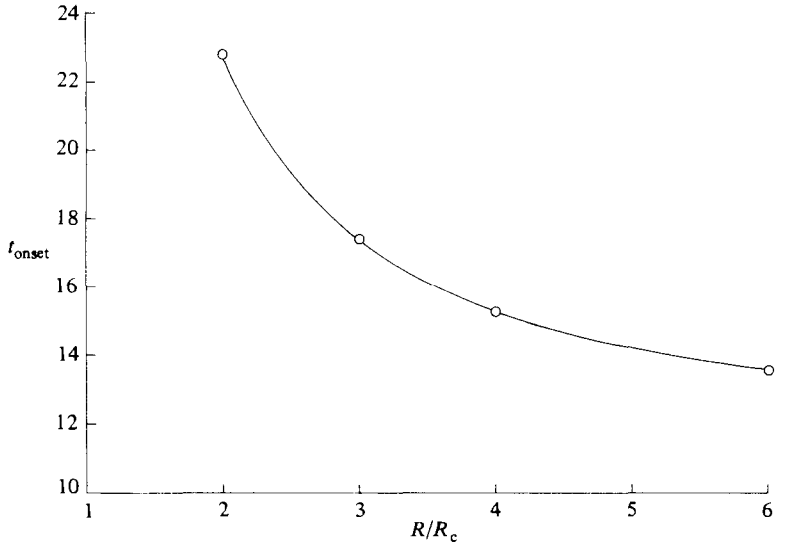

FIGURE 11. Onset time versus R/R_c.

From $A(t)$ it is possible to define an onset time, although it is difficult to justify the use of any definition over any other with the occurrence of events like spontaneous nucleation and vortex-front propagation. We choose to define the onset time to be that time when $A(t)$ has reached 1/e of its equilibrium value A_e, where we shall approximate A_e by the last computed value of $A(t)$. Obviously, for $R/R_c = 1.03$ and $R/R_c = 6$, $A(t)$ is far from reaching A_e, so the results for these two cases will be very imprecise. For the other cases, however, the results should be reasonable. The onset times computed using this definition are listed in table 1 in terms of four different timescales:

$$t_\Omega = t'\Omega \quad \text{(rotational)},$$

$$t_D = \frac{t'\nu}{d^2} \quad \text{(diffusive)},$$

$$t_B = \frac{4(\nu t')^{\frac{1}{2}}}{d} \quad \text{(boundary-layer)},$$

$$t_E = t'\Omega\gamma^{-1}R^{-\frac{1}{2}} \quad \text{(Ekman)}.$$

The diffusive time t_D is representative of the timescale over which the basic state would develop in an infinitely long cylinder, t_B is a measure of the impulsively generated (Rayleigh) boundary-layer thickness, and t_E is an Ekman timescale associated with the spin-up time (Greenspan 1968) of a finite-length system.

t_B is related to a Görtler parameter (Neitzel & Davies 1981) which has been used to correlate data for flow over concave walls, while t_E might be useful if the flow at the midplane is strongly affected by Ekman pumping at the endwalls. Since onset does not occur at a fixed value for any of these scales, there appears to be no advantage in choosing one over another. Notice also, that the equilibrium amplitude A_e for the midplane vortex shows no apparent trend with R/R_c.

The results for $2 \leqslant R/R_c \leqslant 6$ have been plotted in terms of t_Ω in figure 11. While no quantitative results are available for comparison, the trend of the results is in

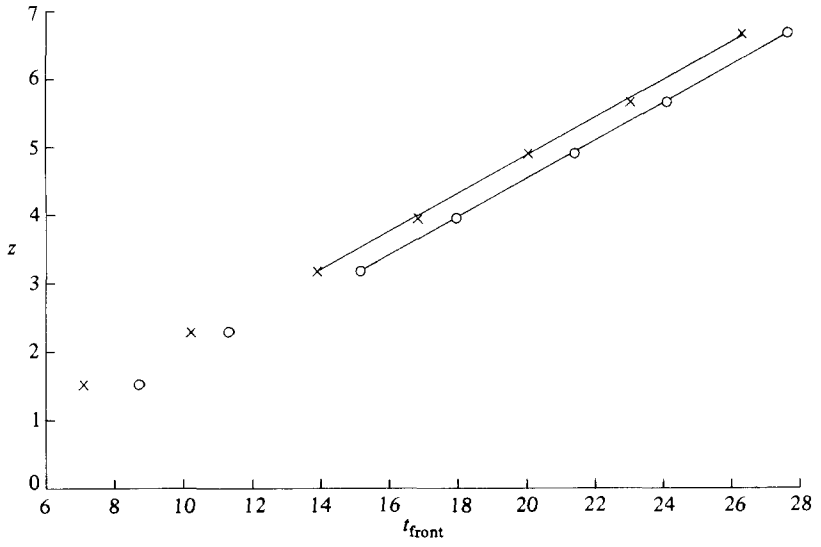

FIGURE 12. Vortex-front position versus time for $R/R_c = 2$: ×, 10%; ○, 20%.

qualitative agreement with the wide-gap ($\eta = 0.1$) results of Kirchner & Chen (1970); onset time decreases monotonically with increasing R/R_c.

A recent paper by Ahlers & Cannell (1983) discusses the onset of instability in finite-length circular Couette flow in terms of a vortex 'front' propagating from the ends of the apparatus into the interior. Their experiments were performed by impulsively increasing the Reynolds number from subcritical to supercritical values as measured by $\epsilon = R/R_c - 1$. The initial conditions were steady state at $\epsilon_0 = -0.2$, and final states ranged from $\epsilon_1 = 0.01$ to $\epsilon_1 = 0.1$. Kalliroscope particles were employed for flow visualization, and the vortex-front arrival time for a given axial location was determined by a specified percentage change in the reflectance at that point. The vortex-front velocity was found to be consistent with, although much smaller than, a prediction resulting from a hypothesized amplitude equation.

To investigate this phenomenon for the strongly nonlinear cases treated here, we can monitor the axial (or radial) velocity near the point of its maximum value within a known vortex, and when this velocity reaches a specified percentage of its own equilibrium value then the front is deemed to have arrived at that point. Ahlers & Cannell (1983) state that the choice of the percentage influences only the arrival time, but not the resulting front velocity. This is not entirely true, since both the reflectance and the axial velocity are representative of disturbances, which are growing in a nonlinear fashion. This nonlinearity may vary spatially and therefore change the arrival times by more than a constant amount. We computed arrival times based on achievement of 10% and 20% of the equilibrium axial velocity. The resulting front velocities were found to vary slightly, but by an amount which would probably be buried in any experimental noise.

Figure 12 is a plot of position versus front arrival time for $R/R_c = 2$. The first-selected position was near the axial centre of the vortex adjacent to the end cell. Computations were not taken to the midplane owing to the nucleation effects discussed earlier. Front velocities were computed from the slopes of least-squares fits through a range of four or five data points over which the velocity appeared to be constant and unaffected by nucleation near the midplane. The results for the

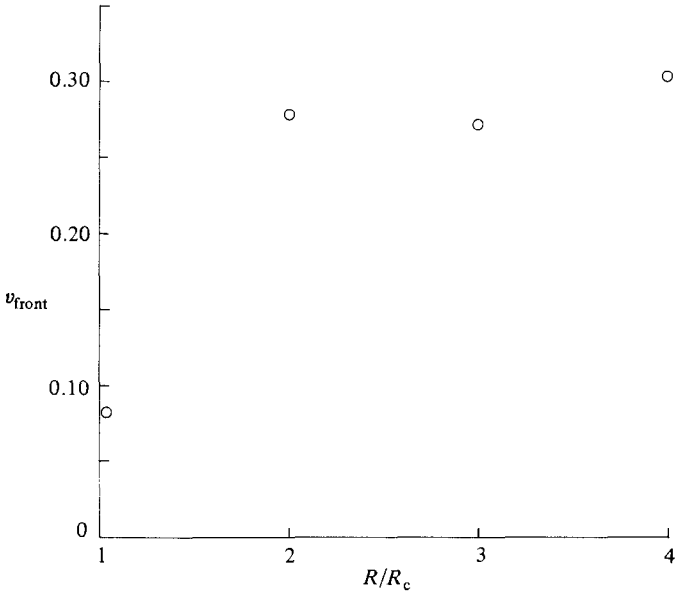

FIGURE 13. Mean vortex-front velocity versus R/R_c.

$\gamma = 23.35$ cases in the range $1.03 \leqslant R/R_c \leqslant 4$ are shown in figure 13. The front velocity is low for $R/R_c = 1.03$, but increases by a factor of 3 for the other cases, indicating an onset which would appear to be more nearly instantaneous to an observer of a flow-visualization experiment. In terms of the notation of Ahlers & Cannell, our result for $R/R_c = 1.03$ corresponds to $\log_{10}\epsilon_1 = -1.52$ with $\log_{10}(v_{\text{front}})$ in the range 0.40–0.45 depending on whether one uses a 10 % or 20 % change as the criterion. This result falls on their plot (figure 3 of their paper) bracketing the result from their amplitude equation.

In summary, the numerical experiments described herein have yielded useful information about the instability of a three-dimensional time-dependent basic state within a finite-geometry apparatus. Agreement with laboratory data for the resultant steady-state flows is excellent in the regime where the assumptions of the code (in this case, axisymmetry) are valid. (The present state of computer hardware makes a stimulation of non-axisymmetric flow in a finite-length geometry of this size impractical, and perhaps impossible.) Once the initial computations have been performed and stored on tape or disc, they are readily available for the extraction of any type of results desired. Parameters of the flow (R, η, γ etc.) may be changed at will.

In conclusion, the numerical experiment is indeed a useful tool for the analysis of complex unstable flows whose basic states are steady or unsteady and whose geometries are finite or infinite. The use of a time-dependent formulation based on the full Navier–Stokes equations is valuable for studying not only equilibrium states, but also the nonlinear approach to these states. Such may not be the case for examining the bifurcations and hysteresis observed experimentally by Mullin (1982), which required extremely long settling times; arclength continuation methods of the type employed by Meyer-Spasche & Keller (1980) are probably better suited to this problem.

I wish to thank Prof. D. F. Jankowski and Prof. E. L. Koschmieder for helpful discussions regarding this work. Many of the programming modifications to the original code were made by Mrs Sharilyn M. Johnson while involved with a summer undergraduate research participation program at Arizona State University. This research was supported by the National Science Foundation under Grants CME-8006696 and MEA 8209923.

REFERENCES

AHLERS, G. & CANNELL, D. S. 1983 Vortex-front propagation in rotating Couette–Taylor flow. *Phys. Rev. Lett.* **50**, 1583.

ALONSO, C. V. & Macagno, E. O. 1973 Numerical integration of the time-dependent equations of motion for Taylor vortex flow. *Comp. Fluids* **1**, 301.

ALZIARY DE ROQUEFORT, T. & GRILLAUD, G. 1978 Computation of Taylor vortex flow by a transient implicit method. *Comp. Fluids* **6**, 259.

BENJAMIN, T. B. & MULLIN, T. 1982 Notes on the multiplicity of flows in the Taylor experiment. *J. Fluid Mech.* **121**, 219.

BENTON, E. R. & CLARK, A. 1974 Spin-up. *Ann. Rev. Fluid Mech.* **6**, 257.

BURKHALTER, J. E. & KOSCHMIEDER, E. L. 1974 Steady supercritical Taylor vortices after sudden starts. *Phys. Fluids* **17**, 1929.

COLES, D. 1965 Transition in circular Couette flow. *J. Fluid Mech.* **21**, 385.

DAVIS, S. H. 1976 The stability of time-periodic flows. *Ann. Rev. Fluid Mech.* **8**, 57.

DIPRIMA, R. C. & SWINNEY, H. L. 1981 Instabilities and transition in flow between concentric rotating cylinders. In *Hydrodynamic Instabilities and the Transition to Turbulence* (ed. H. L. Swinney & J. P. Gollub), p. 139. Springer.

DONNELLY, R. J., SCHWARZ, K. W. & ROBERTS, P. H. 1965 Experiments on the stability of viscous flow between rotating cylinders. VI. Finite amplitude experiments. *Proc. R. Soc. Lond.* A **283**, 531.

GREENSPAN, H. P. 1968 *The Theory of Rotating Fluids.* Cambridge University Press.

HOMSY, G. M. 1973 Global stability of time-dependent flows: impulsively heated or cooled fluid layers. *J. Fluid Mech.* **60**, 129.

KIRCHNER, R. P. & CHEN, C. F. 1970 Stability of time-dependent rotational Couette flow. Part 1. Experimental investigation. *J. Fluid Mech.* **40**, 39.

KITCHENS, C. W. 1980 Navier–Stokes solutions for spin-up in a filled cylinder. *AIAA J.* **18**, 929.

LIU, D. C. S. & CHEN, C. F. 1973 Numerical experiments on time-dependent rotational Couette flow. *J. Fluid Mech.* **59**, 77.

MEYER-SPASCHE, R. & KELLER, H. B. 1980 Computations of the axisymmetric flow between rotating cylinders. *J. Comp. Phys.* **35**, 100.

MULLIN, T. 1982 Mutations of steady cellular flows in the Taylor experiment. *J. Fluid Mech.* **121**, 207.

NEITZEL, G. P. 1982*a* Stability of circular Couette flow with variable inner-cylinder speed. *J. Fluid Mech.* **123**, 43.

NEITZEL, G. P. 1982*b* Marginal stability of impulsively initiated Couette flow and spin-decay. *Phys. Fluids* **25**, 226.

NEITZEL, G. P. & DAVIS, S. H. 1981 Centrifugal instabilities during spin-down to rest in finite cylinders. Numerical experiments. *J. Fluid Mech.* **102**, 329.

SNYDER, H. A. 1969 Wave-number selection at finite amplitude in rotating Couette flow. *J. Fluid Mech.* **35**, 273.